Article:
Kim, Y, Schenk, AS, Walsh, D et al. (3 more authors) (2014) Bio-inspired formation of functional calcite/metal oxide nanoparticle composites. Nanoscale, 6. 852 - 859. ISSN 2040-3364

https://doi.org/10.1039/c3nr05081e

Bio-inspired formation of functional calcite/ metal oxide nanoparticle composites

Yi-Yeoun Kim[a]*, Anna S. Schenk[a], Dominic Walsh[b], Alexander N. Kulak[a], Oscar Cespedes[c] and Fiona C. Meldrum[a]*

Biominerals are invariably composite materials, where occlusion of organic macromolecules within single crystals can significantly modify their properties. In this article, we take inspiration from this biogenic strategy to generate composite crystals in which magnetite (Fe_3O_4) and zincite (ZnO) nanoparticles are embedded within a calcite single crystal host, thereby endowing it with new magnetic or optical properties. While growth of crystals in the presence of small molecules, macromolecules and particles can lead to their occlusion within the crystal host, this approach requires particles with specific surface chemistries. Overcoming this limitation, we here precipitate crystals within a nanoparticle-functionalised xyloglucan gel, where gels can also be incorporated within single crystals, according to their rigidity. This method is independent of the nanoparticle surface chemistry and as the gel maintains its overall structure when occluded within the crystal, the nanoparticles are maintained throughout the crystal, preventing, for example, their movement and accumulation at the crystal surface during crystal growth. This methodology is expected to be quite general, and could be used to endow a wide range of crystals with new functionalities.

Introduction

Advances in technology demand an ever-increasing degree of control over material structure, properties and function. As the range of properties that can be obtained from monolithic materials is necessarily limited, one potential strategy for the development of new materials is the creation of composites in which two or more dissimilar materials are combined. The field of composite materials is clearly well-established, and many approaches have been used to create new materials which profit from the unique features of each component. For example, the strength and conductivity of carbon nanotubes have been exploited in polymer composites,[1] while combination of clay particles with polymers offers excellent mechanical and barrier properties.[2] However, while the formation of many composites relies on the application of high temperatures, non-aqueous solvents and complex processing methods, a beautiful demonstration that mineral-based

composites can be fabricated under ambient conditions and in aqueous solutions is provided by biominerals such as bones, teeth and seashells.[3] These materials are structurally complex, and show many unique features,[4] such as exceptional hardness and toughness, which can be attributed to their inorganic/ organic composite structure where organic species, in the form of isolated macromolecules or fibres, are intimately associated with the mineral phase.[5-8]

In the work described here, we use biominerals, and specifically their occlusion of organic species, as an inspiration to generate composites in which inorganic nanoparticles (magnetite and ZnO) are incorporated within single crystals of calcite ($CaCO_3$). In doing so, we can endow the host crystal with novel properties – here magnetic or optical – while maintaining the intrinsic single crystal character of the parent crystal. It is well recognized that growth of crystals in the presence of organic molecules can lead to the occlusion of both small molecules[9] and macromolecules,[10] and this strategy has been adapted to achieve encapsulation of polymer latexes and copolymer micelles within single crystals of calcite[11, 12] and ZnO crystals.[13] However, while this method is experimentally facile, it requires particles with specific surface chemistries, and aggregation of the nanoparticles is a problem in many crystal growth solutions.

Notably, some biominerals also occlude fibres, reflecting their growth in a gel-like medium.[8, 14, 15] Again, an analogous result has also been achieved synthetically, where sponge-like agarose gels were preserved within calcite crystals.[16, 17] Indeed, incorporation of the gel is subject to far fewer constraints than isolated particles/ molecules, and effective occlusion can be achieved according to the gel rigidity and the rate of crystal growth.[17] Our methodology therefore profits from the ability to occlude gel fibres within single crystals, where pre-functionalisation of the selected gel with inorganic nanoparticles leads to their occlusion within the host crystal. Further, as the gel maintains its gross form when entrapped within the crystal, the locations of the nanoparticles within the crystal are defined, which prevents, for example, migration of the nanoparticles during crystallization and their accumulation at the crystal surface. Importantly, this method circumvents the need to synthesize nanoparticles with specific surface chemistries and has considerable versatility, relying only on the ability to bind inorganic nanoparticles to the gels. It is emphasised that this strategy succeeds in occluding nanoparticles within a single crystal host, rather than the far more common amorphous or porous polycrystalline/ mesocrystal matrices.[18, 19, 20]

Experimental section

Materials

Xyloglucan (Xyg) (MW~60K) (Figure 1) was obtained from Dainippon Sumitomo Seiyaku, Co. Ltd., Osaka, Japan, while all other materials were obtained from Sigma-Aldrich and used as supplied. Acid-neutral endo-1,4-β-D-xylanase from Trichoderma longibrachiatum (X2629), which shows activity to hemicelluloses including xyloglucan, was used for enzymatic de-shelling of nanoparticles. [21]

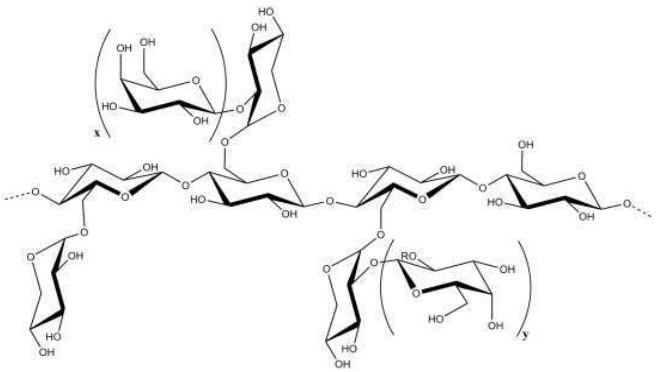

Figure 1. A general molecular structure of xyloglucan.[32]

Preparation of xyloglucan gel functionalised with zinc oxide and magnetite nanoparticles

Nanoparticle functionalised gels were prepared using a method based on our established procedure.[21] Briefly, zinc oxide was synthesised by dissolving $Zn(NO_3)_2.6H_2O$, in a 4 wt% Xyg aqueous solution to give a concentration of 21 mM, where a highly viscous solution was formed. The pH of the solution was adjusted to 12 by adding 1M NaOH solution, and the mixture was stirred and then heated to 80 ^oC in a microwave. The pH was then adjusted to 7 with dilute HNO_3 or HCl solution, while cooling to room temperature in an ice water bath. This mixture was then centrifuged at 5000 rpm for 30 min to remove large aggregated sediments, and the cloudy dark brown magnetite or white zinc oxide supernatant was then collected and dialysed for 2 days to remove residue salts, prior to drying in an oven to obtain the final nanoparticle-Xyg biopolymer products. Magnetite was synthesised using the same method, but substituting 7 mM $FeCl_2.4H_2O$ and 14 mM $FeCl_3.6H_2O$ for the Zn reagent.

In order to effectively analyse the inorganic nanoparticles, the majority of the Xyg polymer coating was removed by enzyme treatment. 0.4 mg/ml of xylanase enzyme was added to 10

mg/ml of nanoparticles-Xyg solution, and the mixture was then left at RT for 2 days. After this time, the inorganic nanoparticles were isolated by light centrifugation and washing with DI water, and were characterised using TEM, XRD, UV and FT-IR. The incorporation of these particles within calcite crystals was also investigated by precipitating $CaCO_3$ in the presence of 100 – 500 µg/ml of these particles.

Precipitation of calcium carbonate within nanoparticle-gels

Dried nanoparticle-Xyg biopolymer was dissolved in DI water to form a viscous gel, and $CaCl_2$ solution was then added to obtain final concentrations of 1-4 wt % gel and [$CaCl_2$] = 5-50 mM. The Ca-infiltrated gel was then transferred to a Petri dish containing cleaned glass slides, and calcium carbonate was precipitated using the ammonium diffusion method or direct addition method.[22] The petri dishes were covered with parafilm, pierced with 3 holes and then placed in a desiccator pre-charged with fresh ammonium carbonate powder or solution. Crystallisation was typically allowed to proceed overnight. Afterwards, the fully-grown crystals were isolated from the gel phase by thoroughly dissolving the gel in DI water, finally rinsing them in ethanol and air-drying.

Characterization of $CaCO_3$/ inorganic nanoparticle-gel composites

The $CaCO_3$ precipitates were characterised using a range of analytical techniques including Scanning electron microscopy (SEM), Transmission Electron Microscopy (TEM), high resolution TEM (HRTEM), thermogravimmetric analysis (TGA), powder XRD (PXRD), Atomic absorption spectroscopy (AAS) and Raman microscopy. Crystal morphologies were characterised using SEM by mounting the glass slides supporting the $CaCO_3$ crystals on SEM stubs using adhesive conducting pads and coating with Pt/Pd. Imaging was performed using a LEO 1530 Gemini FEG-SEM operating at 3 kV using an in-lens detector mode. The cross-sections of particles were imaged using SEM to investigate gel and nanoparticle occlusion, where fractured particles were prepared by placing a clean glass slide on top of the glass slide supporting the calcite crystals, and pressing down, thereby fracturing the crystals. TEM and EDXA were carried out using a FEI Tecnai TF20 FEGTEM Field emission gun TEM/STEM fitted with an HAADF detector, an Oxford Instruments INCA 350 EDX system/80mm X-Max SDD detector and a Gatan Orius SC600A CCD camera, operating at 200 kV.

The location of nanoparticles within the calcite crystal was also studied using HRTEM of thin sections prepared by Focused Ion Beam milling (FIB). FIB to electron transparency was

performed using an FEI Dual Beam system equipped with a 30kV Ga-beam and a field emission electron gun operating at 5 kV. Prior to milling, the samples were thinned by mechanically polishing calcite crystals embedded in TEM epoxy resin.

The individual crystal polymorphs were confirmed with Raman microscopy, using a Renishaw Raman 2000 System Microscope operating with a 785 nm laser, and polymorphs of bulk crystals were also confirmed with powder XRD using a Bruker D8 Advanced diffractometer equipped with an X-ray source emitting Cu $K\alpha_1$ radiation. Samples were placed on a piece of silicon wafer, and XRD data were collected in an angular range between 5 ^{o} and 70 ^{o} in intervals of 0.02^{o}, with a scan rate of 1^{o} min^{-1}. The composition of the crystals grown in the gels was analysed using a TA-Instruments SDT Q600 Simultaneous TGA/DSC, with the analysis being performed under air and N_2 gas in the temperature range from ambient to 850 °C with a heating rate of 5 °C/min. The composite crystal samples were dissolved in 5 % nitric acid and analyzed using a Perkin-Elmer Atomic Absorption Spectrometer, AAnalyst 400 with air-acetylene flame, to obtain the content of Fe (for calcite/ Fe_3O_4-gel) and Zn (for calcite/ZnO-gel).

The magnetic properties of the calcite/ Fe_3O_4-gel composites were measured using an Oxford Instruments Vibrating Sample Magnetometer (VSM) operating at temperatures from 3 K to room temperature. To investigate the optical properties of the calcite/ZnO-gel composite crystals, the samples were placed in disposable cuvettes (path length 10 mm) and analysed using a Perkin-Elkin Lambda 35 system operating at a slit width of 1.0 nm.

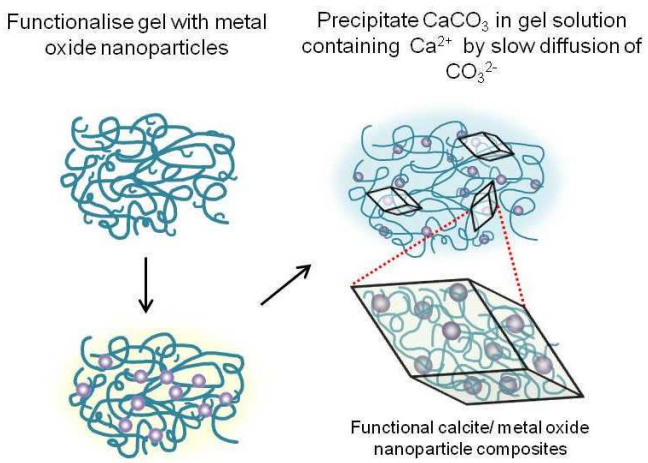

Figure 2: Schematic diagram of the methodology used to generate functional calcite/ metal oxide nanoparticle composites.

Results

Calcite crystals were precipitated within a bio-polymer (xyloglucan) gel functionalised with magnetite nanoparticles to generate composites in which the nanoparticles are distributed throughout the parent host. Calcite was selected as the host crystal based on its ability to occlude foreign material within the crystal lattice,[4, 12, 17] while the magnetite nanoparticles as provide contrasting sizes, morphologies, composition and function. The gels, in turn, were prepared from the biopolymer xyloglucan (Xyg) (Figure 1), which is a soluble hemicellulose polysaccharide from which viscous aqueous gels can be prepared at concentrations of a few wt%. Further, as a waste biopolymer material with demonstrated biocompatibility, Xyg also offers attractive economic and environmental features.

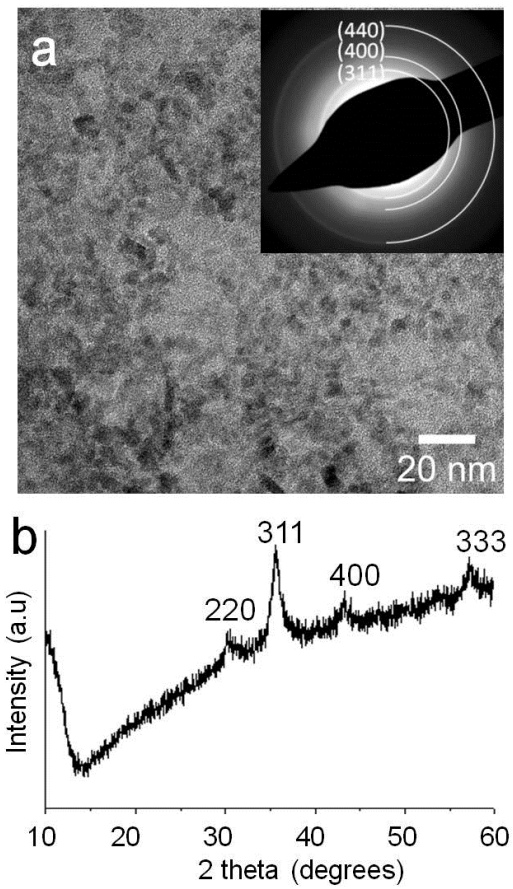

Figure 3: (a) TEM images and corresponding electron diffraction patterns of synthesized magnetite nanoparticles after enzyme treatment and (b) the corresponding XRD pattern.

A Schematic diagram of the methodology used is shown in Figure 2. Stable Xyg gels functionalized with iron oxide nanoparticles were synthesized using a modification of our

established procedure,[21] where the nanoparticles were precipitated in the presence of Xyg, before being purified to remove excess ions and dried. Rehydration of the Xyg-nanoparticles then generated the nanoparticle-functionalized Xyg gels. Characterization of these inorganic nanoparticles using TEM, electron diffraction and X-ray diffraction (Figure 3) showed that the iron oxide particles were magnetite (Fe_3O_4) and that they were roughly spherical in shape and ~ 5 nm in diameter. These dried Xyg-nanoparticles were the used to prepare 4 wt% Xyg-nanoparticle gels by mixing with $CaCl_2$ solutions.

$CaCO_3$ was precipitated within these Fe_3O_4-functionalised Xyg gels (Fe_3O_4-gel) by exposure to ammonium carbonate vapour.[22] Subsequent isolation of the crystals showed that they were calcite, as confirmed by Raman microscopy and powder XRD (Figure S1), and that they were ~20 μm in size and exhibited the well-defined rhombohedral morphologies characteristic of calcite single crystals (Figure 4a). The crystals had slightly truncated edges and rough surfaces, as is typical of gel-grown crystals.[23] These results were compared with control experiments in which calcium carbonate was precipitated within gels of xyloglucan alone, and similar calcite crystals with rough surfaces were produced (Figure S2). That large, rhombohedral crystals of calcite were produced in these xyloglucan-based gels is expected as this biopolymer is functionalized with hydroxyl groups which do not interact strongly with growing $CaCO_3$ crystals.

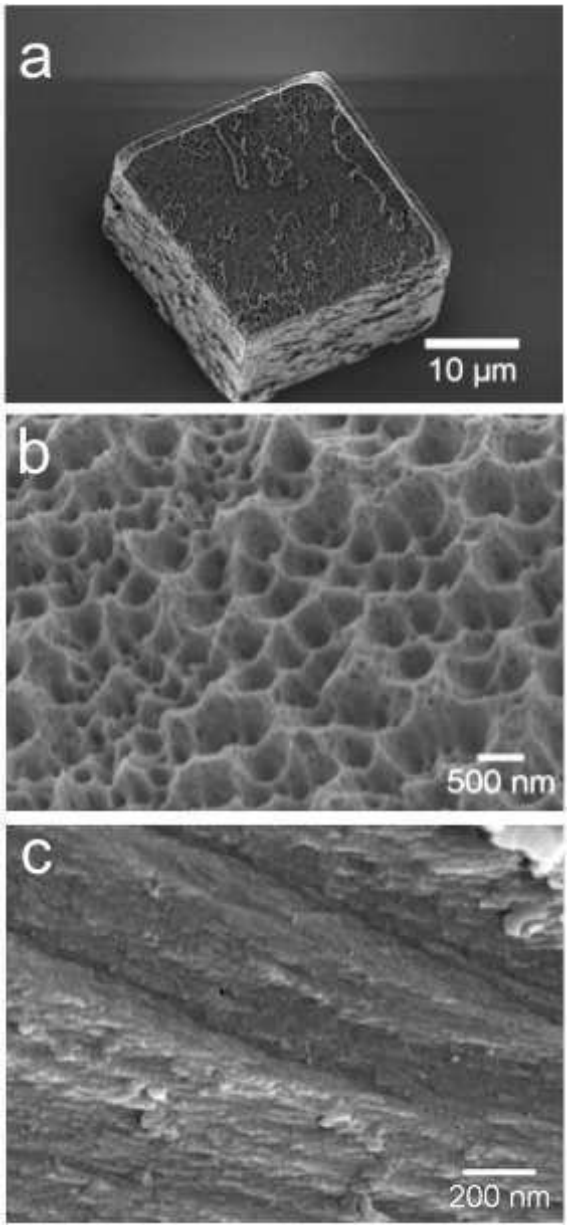

Figure 4. SEM images of calcite/Fe_3O_4-gel crystals. (a) A calcite/Fe_3O_4-gel crystal showing roughened surfaces, (b) an EDTA etched crystal revealing the occluded gel and (c) the cross section of a fractured crystal.

The gel-grown crystals were then analyzed to investigate the incorporation of the metal nanoparticles. Atomic absorption spectroscopy (AAS) was performed to provide a quantitative measure of the amount of nanoparticles entrapped, where the crystals were etched using EDTA solution and water prior to dissolution for analysis by AAS, to remove any nanoparticles/gel adsorbed to the crystal surface. This showed that the calcite/Fe_3O_4-gel composite contained 1.8 wt% Fe_3O_4. Thermogravimetric analysis (TGA) of the same sample gave consistent values,

where the amounts of nanoparticles entrapped within the calcite crystals were estimated as ~2 wt% for Fe_3O_4 through comparison with control samples of Xyg

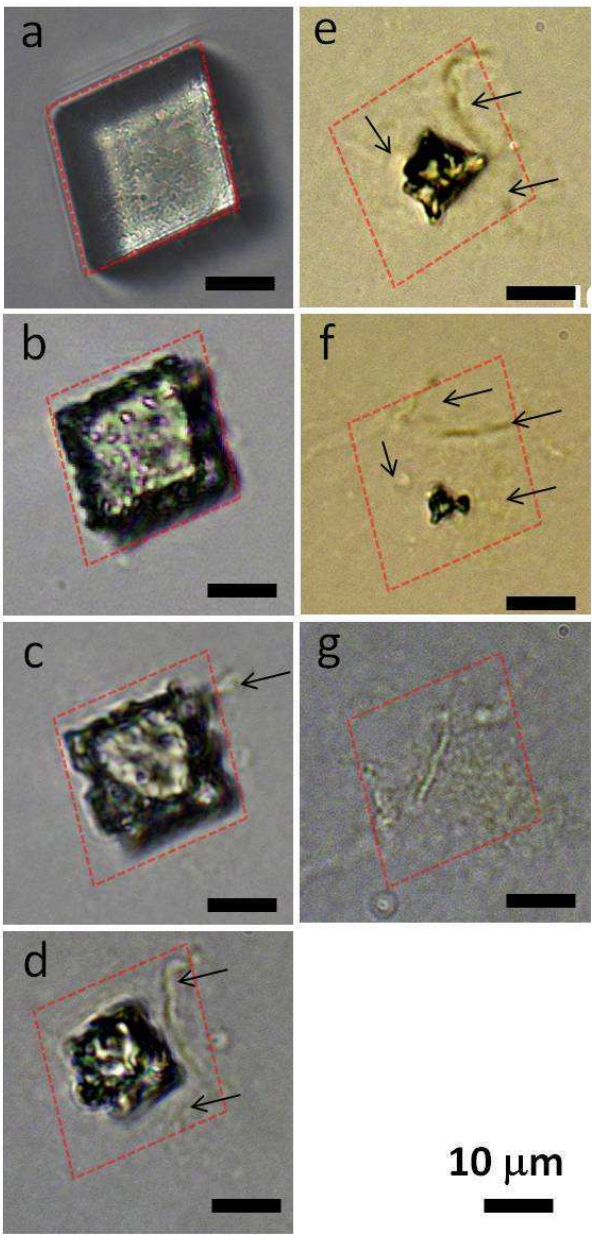

Figure 5. Optical microscope images obtained during dissolution of a calcite/ Fe_3O_4-gel composite crystal with EDTA solution. (a) intact calcite/ Fe_3O_4-gel composite crystal and after dissolution for (b) 9 mins, (c) 14 mins, (d) 21mins, (e) 23 mins, (f) 26 mins and (g) 31 mins.

alone and nanoparticle-functionalized Xyg gels. A full discussion of the data, which is shown in Figures S3 and S4, is provided in the SI. Conclusive demonstration that efficient occlusion of nanoparticles within the calcite crystals occurs due to their attachment to the gel was obtained by precipitation of $CaCO_3$ in the presence of freely-dispersed Xyg-coated nanoparticles. Here, the

Xyg-coated nanoparticles were firstly enzyme-treated to remove the majority of the gel, thereby generating water-soluble nanoparticles that are coated with a only thin shell of Xyg.[21] Analysis of these $CaCO_3$ crystals using SEM, AAS and TGA showed that negligible particles were occluded within them.

The distribution of the gel and nanoparticles within the calcite crystals was investigated by imaging whole crystals, and crystals which had been fractured to expose an internal surface. Treatment of the composite crystals with 0.05 mM EDTA solution for 1~2 hours selectively removed the $CaCO_3$, exposing gel with a characteristic, cell-like structure, uniformly distributed throughout the crystal (Figure 4b). Slow dissolution of a calcite/Fe_3O_4-gel crystal was also followed by *in situ* observation using optical microscopy, where gradual loss of the orange Fe_3O_4-gel was observed (Figure 5). These results can be compared with those obtained by etching pure calcite crystals precipitated in additive-free solution, where etching only leads to a decrease in crystal size, and the development of typical etch pits on the crystal faces (Figure S5). Due to the small sizes (~5 nm) of the magnetite nanoparticles, they could not be identified in SEM analysis of fracture surfaces (Figure 4c). It is interesting to note, however, that the fracture surfaces were much rougher than those characteristic of pure calcite (Figure S6) or calcite grown in the presence of freely-dispersed nanoparticles (Figure S7), which is indicative of a uniform distribution of occlusions throughout the crystal.[11, 12]

The crystals were also studied using Transmission Electron Microscopy (TEM) and specimens thin enough for analysis were prepared by grinding the crystals or by cutting a section with a Focused Ion Beam (FIB) (Figure 6a and 6b). Analysis of the ground calcite/Fe_3O_4-gel particles showed that ~5 nm magnetite nanoparticles were distributed throughout the calcite crystal and selected area electron diffraction (SAED) yielded a single crystal calcite pattern on which diffraction rings corresponding to magnetite were superimposed (Figures 6a inset). This was also supported again by Energy Dispersive X-Ray Analysis (EDXA), which showed the clear presence of Fe throughout the thin-section (Figure 6c).

Having determined that precipitation of crystals within a nanoparticle-gel is an effective route for the production of composites in which the nanoparticles and gel components are distributed throughout the host crystals, the physical properties of the composite samples were themselves investigated. The magnetic properties of the calcite/Fe_3O_4-gel composites were determined using a Vibrating Sample Magnetometer (VSM) at temperatures from 3–298 K. The experiments

revealed that the samples are superparamagnetic at room temperature and ferrimagnetic at low temperatures, and that the magnetic moment at fields of 2 T was in the order of 2 memu, giving a magnetization of 1-2 emu/g. The bulk saturation magnetization of magnetite is 92 emu/g, in good agreement with the estimated magnetite concentration in calcite crystals of 2 wt% (Figures 7a and 7b). A coercive field of ~ 20 mT and a blocking temperature of 42 K, which corresponds to a particle size of ≈ 5 nm, provided a further indication of a uniform distribution of magnetite nanoparticles within the composite crystals.

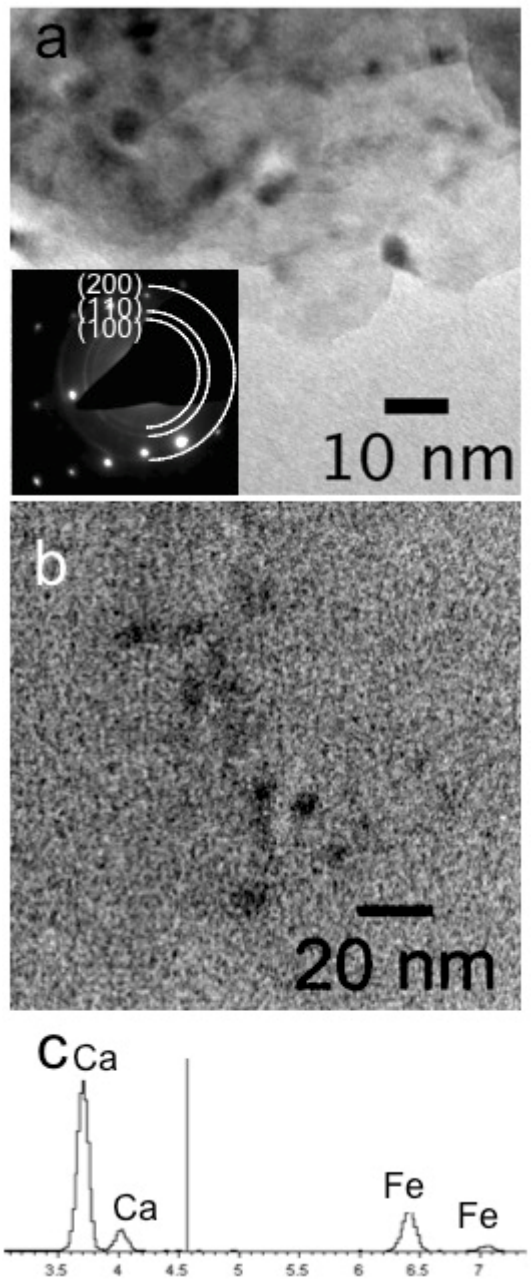

Figure 6. (a) TEM image and corresponding electron diffraction patterns of a ground calcite/Fe_3O_4-gel crystal which shows a single crystal pattern of calcite and rings from the Fe_3O_4 nanoparticles. (b) TEM image of a FIB-sectioned surface and (c) the corresponding EDX spectrum showing the presence of Ca and Fe.

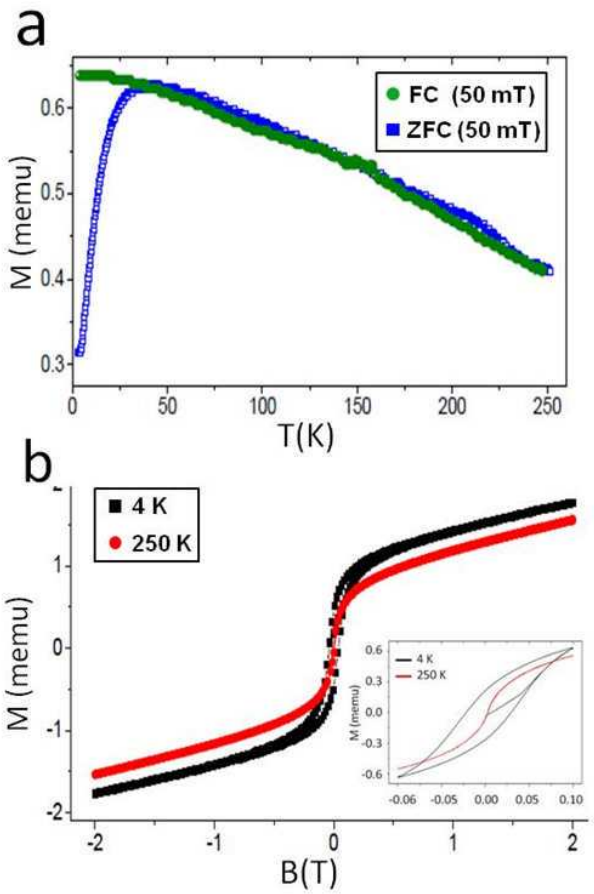

Figure 7. (a) Thermomagnetic Zero-field-cooled/ Field-cooled (ZFC/ FC) curve of calcite/Fe_3O_4-gel crystals and (b) a magnetisation loop of calcite/Fe_3O_4-gel crystals measured at 4K and 250 K. The inset shows the hysteresis loop near the zero-magnetic-field region.

The potential of using the same method to introduce a different functionality into calcite single crystals was also explored. ZnO was therefore precipitated in the presence of Xyg, where TEM and electron diffraction showed that the ZnO particles were zincite rods of dimensions 50 nm × 6-8 nm (Figures 8a and 8b). These and often formed in bundles 50-100 nm in length and approximately 30-40 nm in width. In common with the Xyg-gel system, ~10 μm rhombohedral calcite crystals precipitated within the ZnO-gels, as confirmed by Raman microscopy and powder XRD (Figure 8c and Figure S1). Atomic absorption spectroscopy (AAS) showed that the

calcite/ZnO-gel composite crystals comprised 3.9 wt % ZnO, a result consistent with values of ~4 wt% as determined by TGA (Figures S3 and S4). Analysis of the fractured calcite/ZnO-gel crystals with EDX in an SEM confirmed the presence of occluded ZnO particles (Figures 8d and 8e).

ZnO is a semiconductor and exhibits an optical band gap in the UV region at 290-390 nm, making it one of most efficient UV absorbers.[24] The UV/Vis absorption spectrum of the calcite/ZnO-gel composite crystals was recorded and showed a broad absorption with a maximum peak at 354 nm (corresponding to a band gap energy of 3.50 eV) and a steep slope centered at 364 nm; neither calcite nor Xyg absorb in this region (Figure 8f). This compares with the ZnO-gel prior to the occlusion within the calcite crystals, which exhibits a maximum peak at 353 nm and a slope centered at 367 nm. These absorption energies are significantly higher than that of bulk ZnO at 375 nm (3.3 eV) due to quantum confinement effect of nanorod structure of ZnO with diameter of ~ 8 nm.[24] The UV absorption of the composite crystals can therefore be attributed to the ZnO nanoparticles which are dispersed throughout the host calcite crystal.

Discussion

These data clearly demonstrate that growth of crystals within nanoparticles-functionalised biopolymer gels provides an effective method for generating inorganic-based composite materials, thereby endowing the parent crystal with new physiochemical properties. Traditional methods of synthesis of inorganic/ inorganic composites, such as mechanical mixing followed by annealing, generally lead to rather poor control over microstructure. Greater control can be achieved using more complex processing such as formation of alternate layers using physical deposition or chemical solution processing.[25] Alternatively, inorganic nanoparticles can be embedded within an inorganic matrix, for example by the *in situ* growth of nanoparticles within porous media such as zeolites,[26] the construction of mesoporous solids in the presence of nanoparticles,[27] adsorption of nanoparticles into porous crystals,[28] the formation of discrete core-shell nanoparticle composites,[29] and *in situ* growth of nanoparticles during thin film formation.[30] It is emphasized that in creating these composite materials, there is a requirement not only to succeed in embedding nanoparticles within the host matrix, but to control their density and distribution.

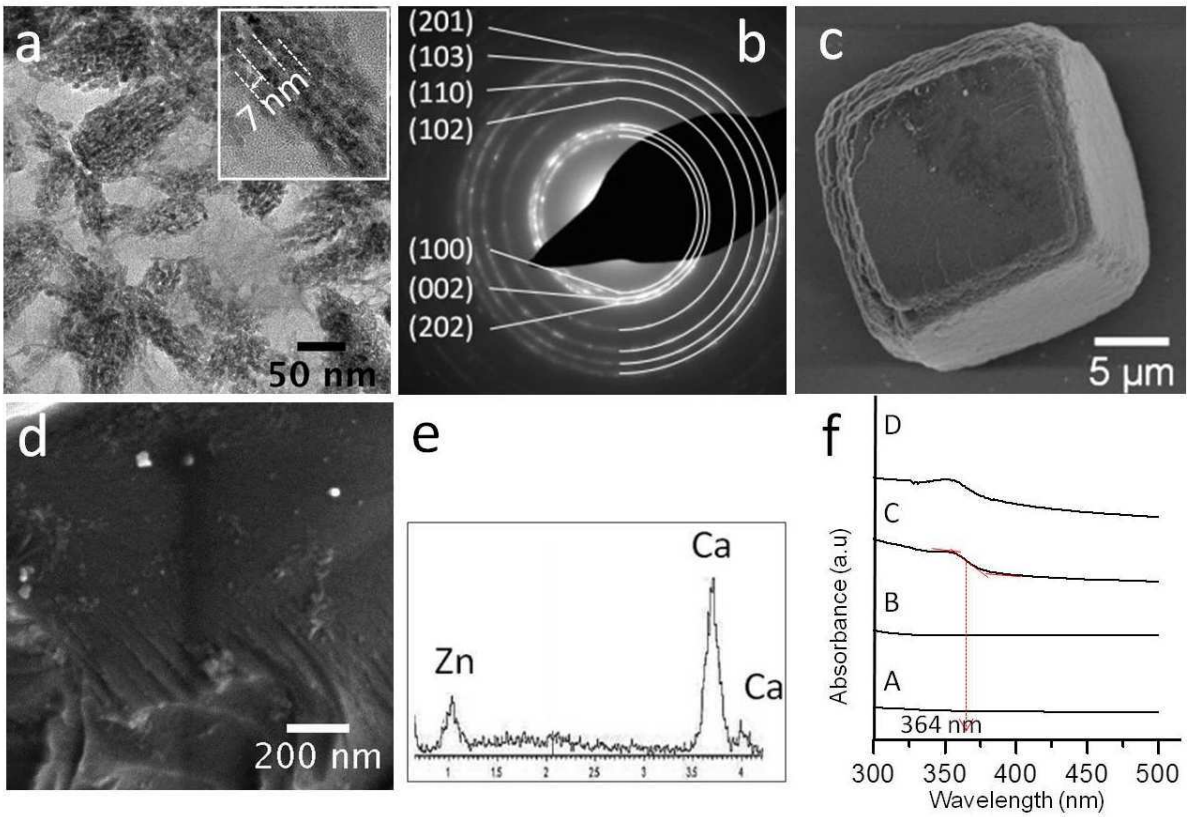

Figure 8. TEM images and corresponding electron diffraction patterns of synthesized (a) Zinc oxide nanoparticles after enzyme treatment and (b) the corresponding electron diffraction pattern. SEM images of (c) calcite/ZnO-gel crystals (d) and their fractured cross section. (e) The corresponding EDX spectrum shows the presence of Zn and Ca. (f) UV-vis absorption spectra of A. Xyg-gel, B. calcite, C. calcite/ ZnO-gel crystals and D. ZnO-Xyg nanoparticles.

In the method employed here, the gel matrix plays multiple roles in directing the structure of the product material. From controlling the formation of the nanoparticles, it then provides a framework on which they are supported, it prevents their aggregation during crystallization and ensures that they are distributed throughout the parent crystal. Association of the nanoparticles with the gel also serves to significantly increase the quantity of gel that is occluded within the calcite crystals. Indeed, 3-5 wt% of Xyg is incorporated in the absence of nanoparticles, while 12 wt% are occluded when the gel is functionalised by magnetite. These values can also be compared with those given for the incorporation of agarose gel in calcite single crystals, where a maximum value of 0.9 wt% was reported for growth in a 1.0 wt/vol% gel.[17] Such occlusion behavior may be related to changes in the rigidity of the gel. Indeed, studies of calcite

precipitation in agarose gels has shown that incorporation is optimised in rigid gels at high growth rates, where the gel network is strong enough to resist the "crystallization pressure" exerted by the growing crystal.[17] Our system may therefore exhibit a synergistic relationship between the gel and nanoparticle occlusion, where functionalization of the Xyg biopolymer with inorganic nanoparticles significantly increases its rigidity, thereby leading to higher incorporation of the biopolymer gel and associated nanoparticles. This is supported by recent studies which have reported that inorganic nanoparticles can act as multifunctional cross-linkers, leading to mechanical reinforcement of hydrogels.[31]

Conclusions

In conclusion, we have described a novel synthetic route – where crystals are precipitated in a nanoparticle-functionalised gel – to generate a composite crystal comprising inorganic nanoparticles within an inorganic single crystal. As model systems we have employed calcite as the host crystal, together with magnetite or zinc oxide nanoparticles located within xyloglucan gels. Further, measurement of the physical properties of the composite crystals demonstrates that this straightforward experimental method leads to integration of the original functionalities of the nanoparticles into the product crystals. Calcium carbonate is widely used in industrial applications for its unique combination of properties, and in developing new applications there is significant current interest in introducing functionality into the crystals. [18, 19, 28] The methodology presented here therefore provides a new and flexible method for constructing $CaCO_3$–based composites, and the successful use of xyloglucan, which is a waste biopolymer material with demonstrated biocompatibility also offers attractive economic and environmental features. It is envisaged that this methodology could be applied to many other systems, potentially leading to new materials and properties, and further work will investigate the generality of the approach.

Acknowledgements

We thank the Engineering and Physical Sciences Research Council (EPSRC) for financial support *via* grant EP/J018589/1 (YYK and FCM), EP/G00868X/1 (AK and FCM) and EP/K006304/1 (AK and FCM). This work was also supported by an EPSRC Leadership Fellowship (FCM and YYK, EP/H005374/1), and an EPSRC Programme Grant (ASS and FCM, EP/I001514/1) which funds the Materials Interface with Biology (MIB) consortium.

Notes and references

[a] School of Chemistry, University of Leeds, Woodhouse Lane, Leeds, LS2 9JT, UK. Email: F.Meldrum@leeds.ac.uk; Y.Y.Kim@leeds.ac.uk. Tel: (0113) 3436414.

[b] Department of Chemistry, University of Bath, Claverton Down, Bath. BA2 7AY, UK.

[c] School of Physics and Astronomy, University of Leeds, Woodhouse Lane, Leeds, LS2 9JT, UK..

† Electronic Supplementary Information (ESI) available: Further analysis of products. See DOI: 10.1039/b000000x/

1. M. Moniruzzaman and K. I. Winey, *Macromolecules*, 2006, **39**, 5194-5205.
2. D. R. Paul and L. M. Robeson, *Polymer*, 2008, **49**, 3187-3204.
3. F. C. Meldrum and H. Colfen, *Chem. Rev.*, 2008, **108**, 4332-4432.
4. H. A. Lowenstam and S. Weiner, *On Biomineralization*, Oxford University Press, New York, 1989.
5. P. Fratzl and R. Weinkamer, *Prog. Mater. Sci.*, 2007, **52**, 1263-1334.
6. B. Pokroy, A. N. Fitch, F. Marin, M. Kapon, N. Adir and E. Zolotoyabko, *J. Struct. Biol.*, 2006, **155**, 96-103.
7. J. Aizenberg, J. Hanson, T. F. Koetzle, S. Weiner and L. Addadi, *J. Am. Chem. Soc.*, 1997, **119**, 881-886.
8. E. Asenath-Smith, H. Y. Li, E. C. Keene, Z. W. Seh and L. A. Estroff, *Adv. Funct. Mater.*, 2012, **22**, 2891-2914.
9. S. Borukhin, L. Bloch, T. Radlauer, A. R. Hill, A. H. Fitch and B. Pokroy, *Adv. Funct. Mater.*, 2012, **22**, 2416-2422.
10. R. A. Metzler, J. S. Evans, C. E. Killian, D. Zhou, T. H. Churchill, N. P. Appathurai, S. N. Coppersmith and P. Gilbert, *J. Am. Chem. Soc.*, 2010, **132**, 6329-6334.
11. Y. Y. Kim, L. Ribeiro, F. Maillot, O. Ward, S. J. Eichhorn and F. C. Meldrum, *Adv. Mater.*, 2010, **22**, 2082-2086.
12. Y. Y. Kim, K. Ganesan, P. C. Yang, A. N. Kulak, S. Borukhin, S. Pechook, L. Ribeiro, R. Kroger, S. J. Eichhorn, S. P. Armes, B. Pokroy and F. C. Meldrum, *Nat Mater*, 2011, **10**, 890-896.

13. R. Munoz-Espi, Y. Qi, I. Lieberwirth, C. M. Gomez and G. Wegner, *Chem. Eur. J.*, 2006, **12**, 118-129.

14. H. Li, H. L. Xin, M. E. Kunitake, E. C. Keene, D. A. Muller and L. A. Estroff, *Adv. Funct. Mater.*, 2011.

15. F. Nudelman, E. Shimoni, E. Klein, M. Rousseau, X. Bourrat, E. Lopez, L. Addadi and S. Weiner, *J. Struct. Biol.*, 2008, **162**, 290-300.

16. H. Y. Li, H. L. Xin, D. A. Muller and L. A. Estroff, *Science*, 2009, **326**, 1244-1247.

17. H. Y. Li and L. A. Estroff, *Adv. Mater.*, 2009, **21**, 470-473.

18. D. Walsh, Y.-Y. Kim, A. Miyamoto and F. C. Meldrum, *Small*, 2011, **7**, 2168–2172.

19. Y. Zhao, Y. Lu, Y. Hu, J.-P. Li, L. Dong, L. Lin and S.-H. Yu, *Small*, 2010, **6**, 2436-2442.

20. M. Mihai, V. Socoliuc, F. Doroftei, E.-L. Ursu, M. Aflori, L. Vekas and B. C. Simionescu, *Crystal Growth and Design*, 2013, **13**, 3535−3545.

21. C. Neudeck, Y. Y. Kim, W. Ogasawara, Y. Shida, F. Meldrum and D. Walsh, *Small*, 2011, **7**, 869-873.

22. J. Ihli, P. Bots, A. Kulak, L. G. Benning and F. C. Meldrum, *Adv. Funct. Mater.*, 2013, **23**, 1965-1973.

23. L. A. Estroff, L. Addadi, S. Weiner and A. D. Hamilton, *Org. Biomol. Chem.*, 2004, **2**, 137-141.

24. Y. W. Chen, Q. Qiao, Y. C. Liu and G. L. Yang, *J Phys Chem C*, 2009, **113**, 7497-7502.

25. C. W. Nan, M. I. Bichurin, S. X. Dong, D. Viehland and G. Srinivasan, *J. Appl. Phys.*, 2008, **103**, 35.

26. J. Dong, Z. H. Xu and S. M. Kuznicki, *Adv. Funct. Mater.*, 2009, **19**, 1268-1275.

27. M. Liong, J. Lu, M. Kovochich, T. Xia, S. G. Ruehm, A. E. Nel, F. Tamanoi and J. I. Zink, *ACS Nano*, 2008, **2**, 889-896.

28. Y. H. Won, H. S. Jang, D. W. Chung and L. A. Stanciu, *J. Mater. Chem.*, 2010, **20**, 7728-7733.

29. W. Schartl, *Nanoscale*, 2010, **2**, 829-843.

30. N. Bahlawane, K. Kohse-Hoinghaus, T. Weimann, P. Hinze, S. Rohe and M. Baumer, *Angew Chem Int Edit*, 2011, **50**, 9957-9960.

31. K. Haraguchi, *Curr. Op. Solid St. Mater. Sci.*, 2007, **11**, 47-54.

32. A. Ebringerova, *Macromol Symp*, 2006, **232**, 1-12.

Supplementary Information

Bio-Inspired Formation of Functional Calcite/ Metal Oxide Nanoparticle Composites

By *Yi-Yeoun Kim*[1]*, *Anna S. Schenk*[1], *Dominic Walsh*[2], *Alexander N. Kulak, Oscar Cespedes*[3] and *Fiona C. Meldrum*[1]*

Analysis of TGA Data

Thermogravimetric analysis (TGA) of the calcite/nanoparticle-gel samples estimated the amounts of nanoparticles entrapped within the calcite crystals as ~ 4 wt% for ZnO and ~ 2 wt% for Fe_3O_4. TGA spectra obtained under nitrogen gas flow showed that the calcite/nanoparticle-gel composites underwent gradual weight loss up to 600 ^oC equal to 4-5 wt % for the calcite-ZnO-gel and 8-9 wt % for the calcite/Fe_3O_4-gel, due to dehydration (1-2 wt%) and degradation of the Xyg polymer (Figure S3). Further heating above 600 ^oC led to decomposition of the $CaCO_3$, and higher amounts of residue were obtained than expected based on the decomposition of pure $CaCO_3$. These excess values over those expected for $CaCO_3$ decomposition alone amounted to ~13 wt % for the calcite/ZnO-gel and ~ 3 wt % for calcite/Fe_3O_4-gel, and can be attributed to entrapped metal oxide nanoparticles and incomplete decomposition of the Xyg polymer. The lower residual for the iron oxide system can be attributed to the fact that the magnetite nanoparticles convert to FeO under heating, which then facilitates decomposition of the biopolymer, even under nitrogen. Therefore, heating to decomposition under nitrogen of the calcite/nanoparticle-gel crystals is accompanied by greater weight loss than would be expected for calcite alone, equal to (5 + 13 = 18 wt%) for the ZnO system and (9 + 3 = 12 wt%) for the Fe_3O_4 system. Given that TGA analysis of the nanoparticle-functionalised Xyg biopolymers under oxygen flow revealed that they comprised ~20 wt% inorganic nanoparticles (Figure S4), the amounts of nanoparticles entrapped within the calcite crystals were estimated as (20% × 18 wt% = ~ 4 wt%) for ZnO and (20% × 12 wt% = ~2 wt%) for Fe_3O_4. These results compare with calcite crystals grown in Xyg-gel (*ie*. in the absence of

inorganic nanoparticles) which under TGA in oxygen shows a weight loss of only 3-4 wt% loss before 600 ^{o}C and stoichiometric decomposition of $CaCO_3$ at 600 ^{o}C (Figure S3).

Figure S1: (A) Raman spectra of calcite/Fe_3O_4-gel and calcite/ZnO-gel composite crystals showing peaks at 1091 or 1090 cm^{-1} (v_1) which correspond to the internal CO_3^{2-} symmetric stretch, a peak at 719 or 717 cm^{-1} (v_4) which corresponds to the CO_3^{2-} symmetric bending mode and lattice mode peaks at 161,289 cm^{-1} and 160,287 cm^{-1} respectively. (B) Powder XRD spectra of calcite/Fe_3O_4-gel and calcite/ZnO-gel composite crystals, where only the strongest (104) peak of calcite was observed due to the limited amounts of samples available.

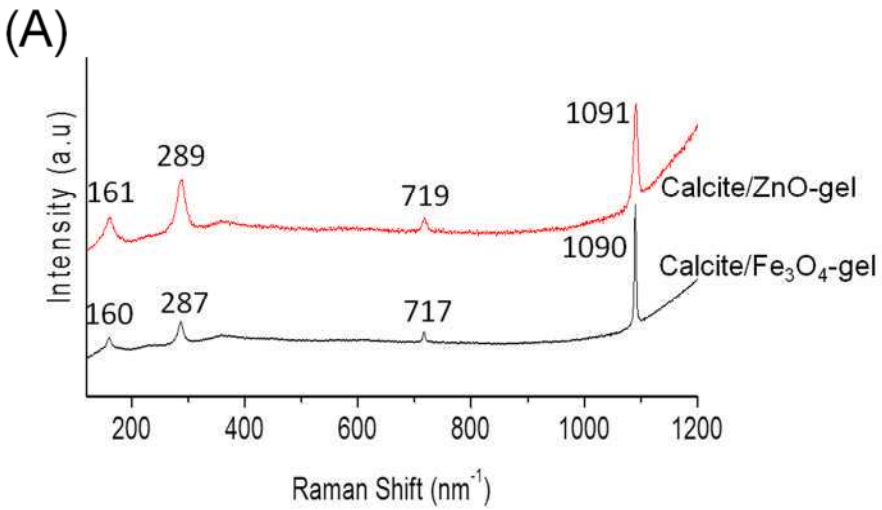

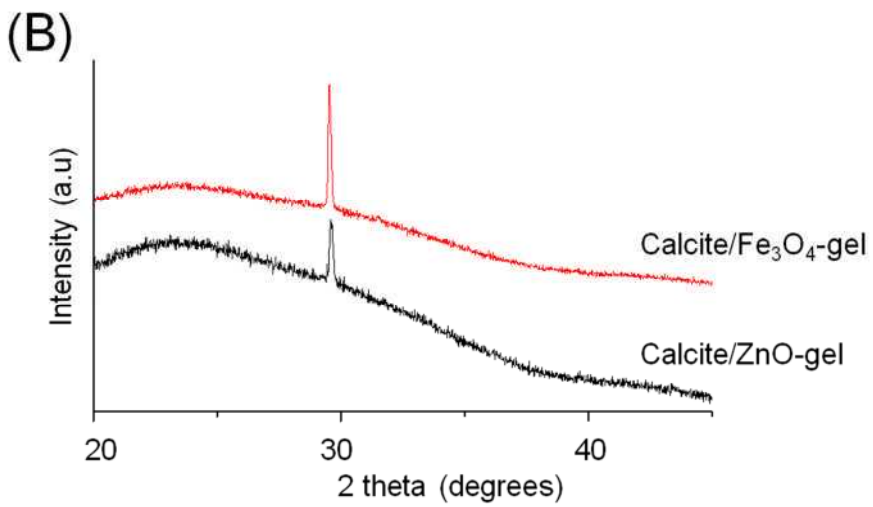

Figure S2. SEM image of a calcite crystal grown in a Xyg gel, showing rough surfaces and slightly truncated edges.

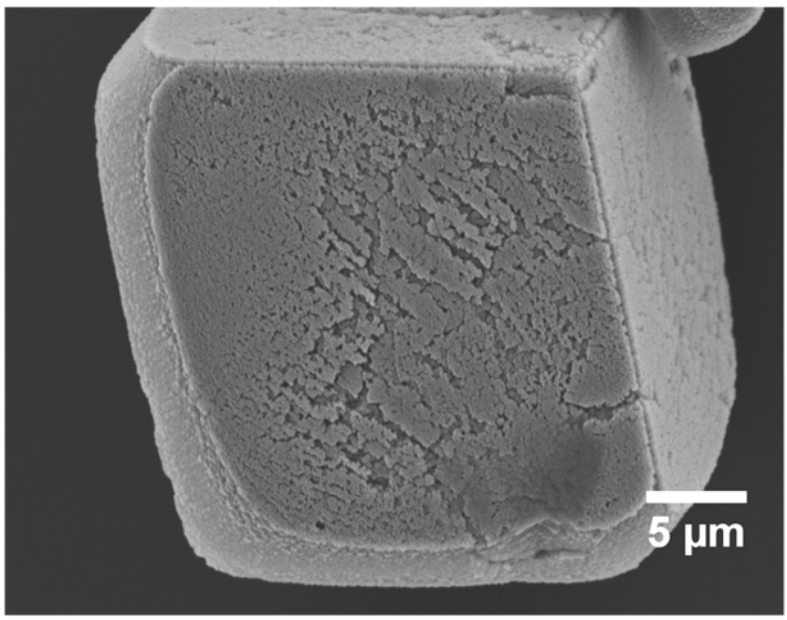

Figure S3. (A) Thermogravimetric analysis (TGA) data of (**a**) Calcite/ZnO-gel and (**b**) Calcite/Fe_3O_4-gel composites. (B) Thermogravimetric analysis (TGA) data of (**a**) pure calcite (red), (**b**) calcite grown in presence of freely-dispersed ZnO nanoparticles (blue) and (**c**) calcite grown within Xyg gel (black). All 3 samples showed stoichiometric decomposition of $CaCO_3$ to CO_2 and CaO (100 $CaCO_3$ →56 CaO + 44 CO_2).

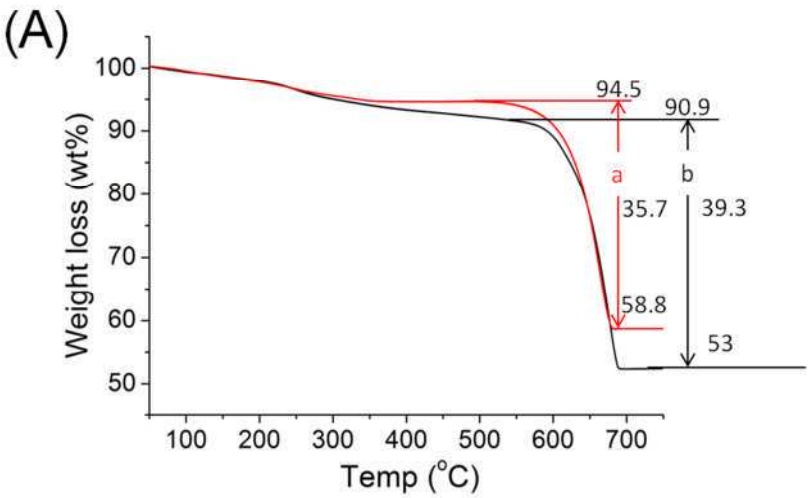

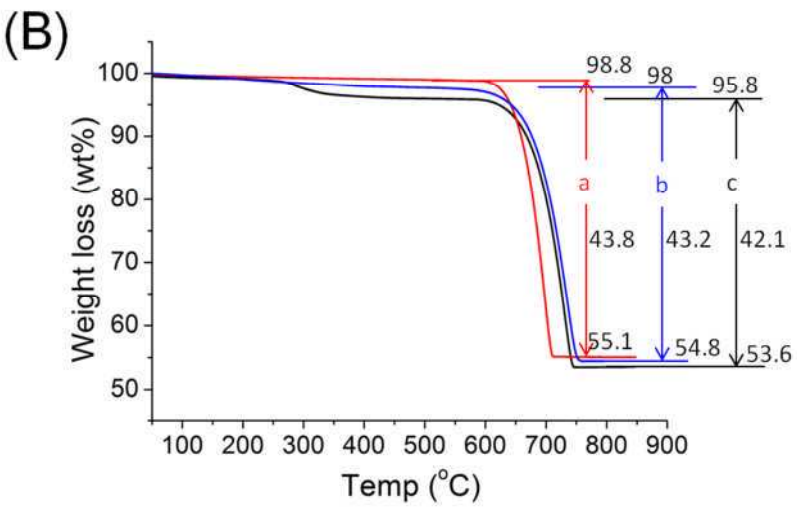

Figure S4. Thermogravimetric analysis data of Xyg biopolymer and Xyg functionalized with Fe_3O_4 and ZnO nanoparticles. Xyg biopolymer fully decomposed before 430 ^oC such that the ~ 20 wt % residue remaining at 500 ^oC could be attributed to Fe_3O_4 or ZnO nanoparticles.

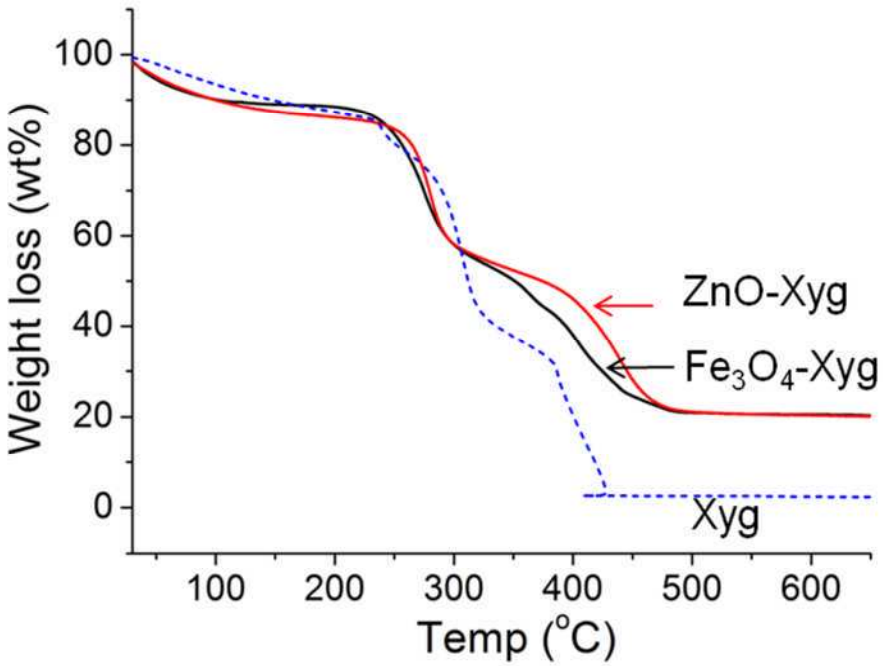

Figure S5. A SEM image of a pure calcite crystal etched with 0.05 M EDTA solution.

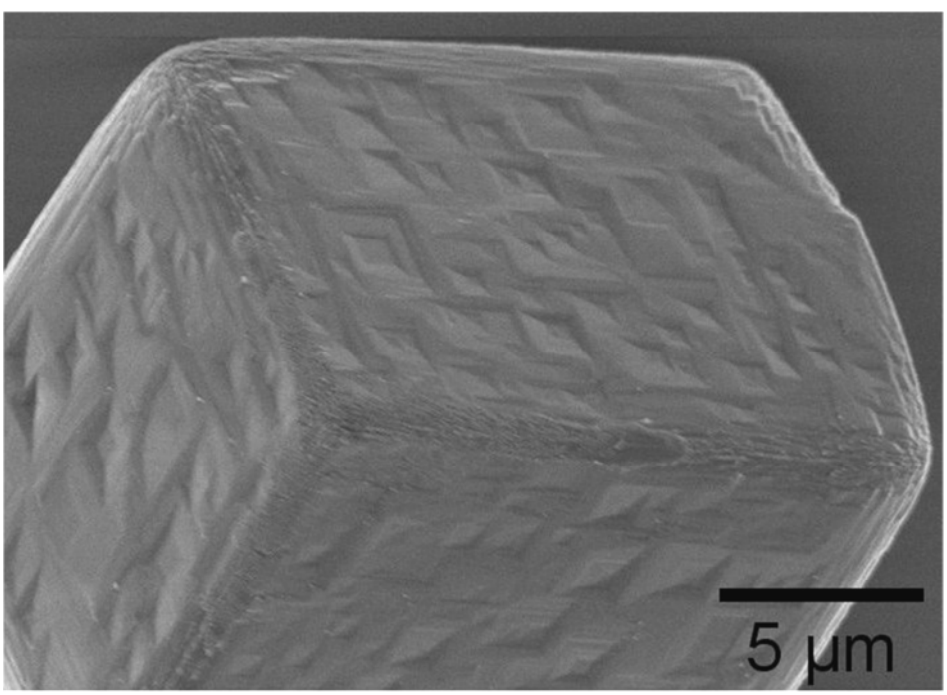

Figure S6. A SEM image of a fractured, pure calcite crystal.

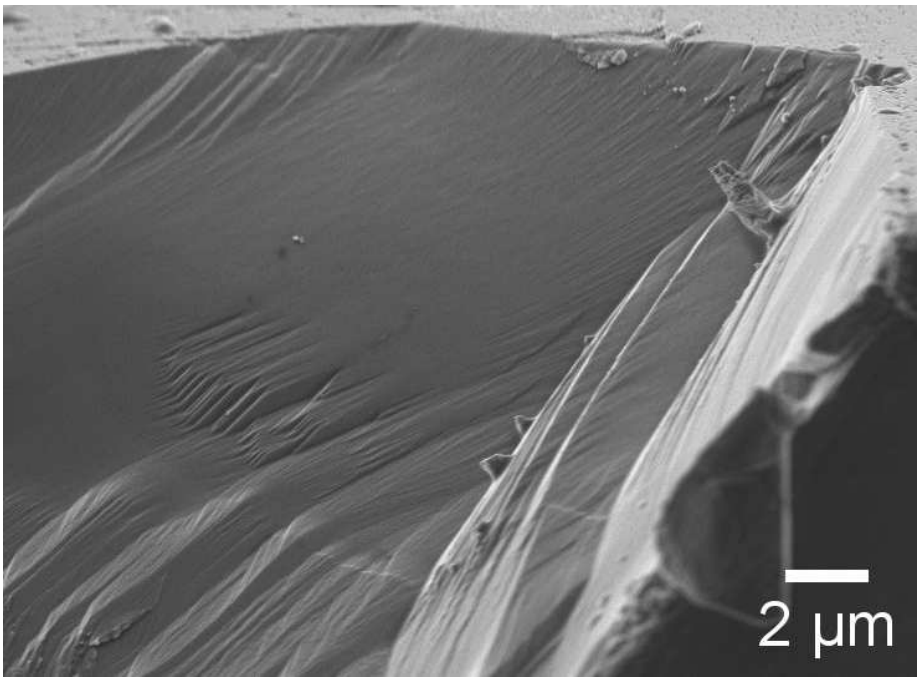

Figure S7. Cross-sections through fractured calcite crystals precipitated in the presence of 100 µg/ml (A) enzyme-treated magnetite nanoparticles and (B) enzyme-treated zinc oxide nanoparticles. Images of intact crystals are shown in the insets.

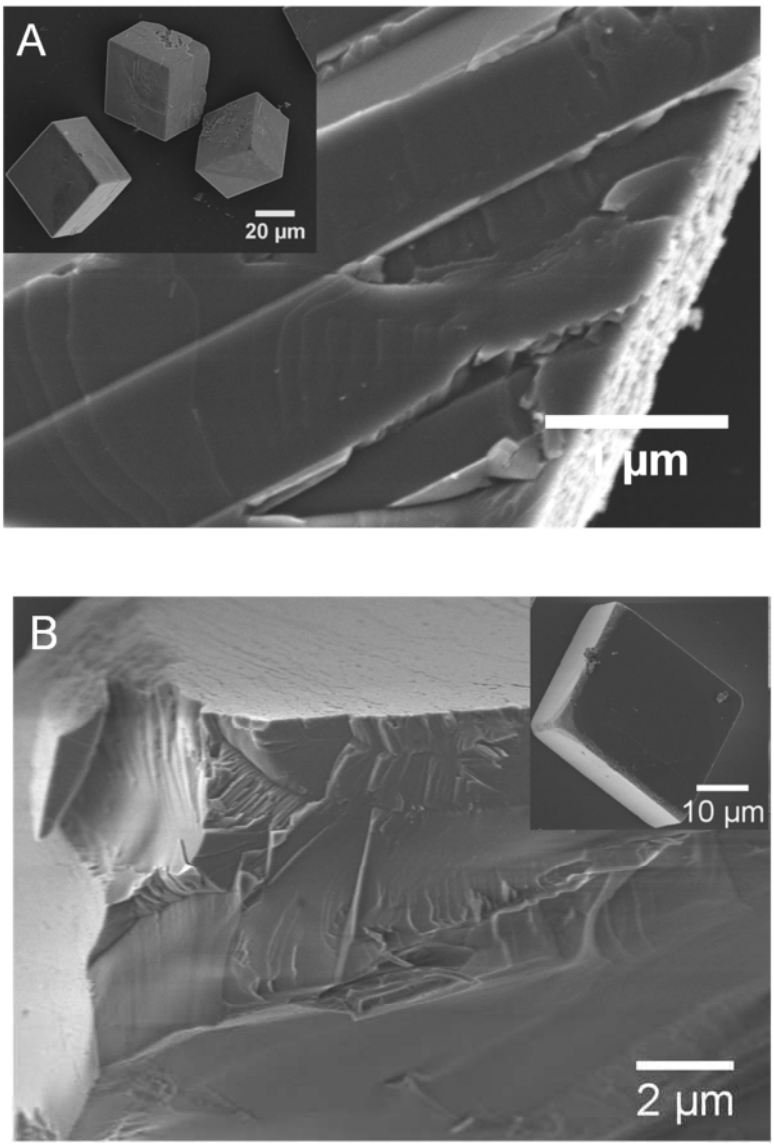

Figure S8. TEM images and corresponding electron diffraction patterns of synthesized (A) magnetite nanoparticles and (B) zinc oxide nanoparticles, after enzyme treatment. XRD spectra and diffraction data of (C) enzyme-treated magnetite nanoparticles and (D) enzyme-treated zinc oxide nanoparticles, and comparison with literature values.